Table S1, related to Figure 1. Microarray analysis of laser captured crypt base epithelial cells from WT and *Nod2*$^{-/-}$ mice.

First tab shows complete gene list where fold change refers to *Nod2*$^{-/-}$ compared to WT. Second tab shows list of genes assigned to the pathways from Figure 1 that were found to be enriched in *Nod2*$^{-/-}$ samples according to DAVID analysis. Third tab shows list of genes that were assigned to the pathways from Fig. S2 according to GSEA analysis.

FIGURE S1

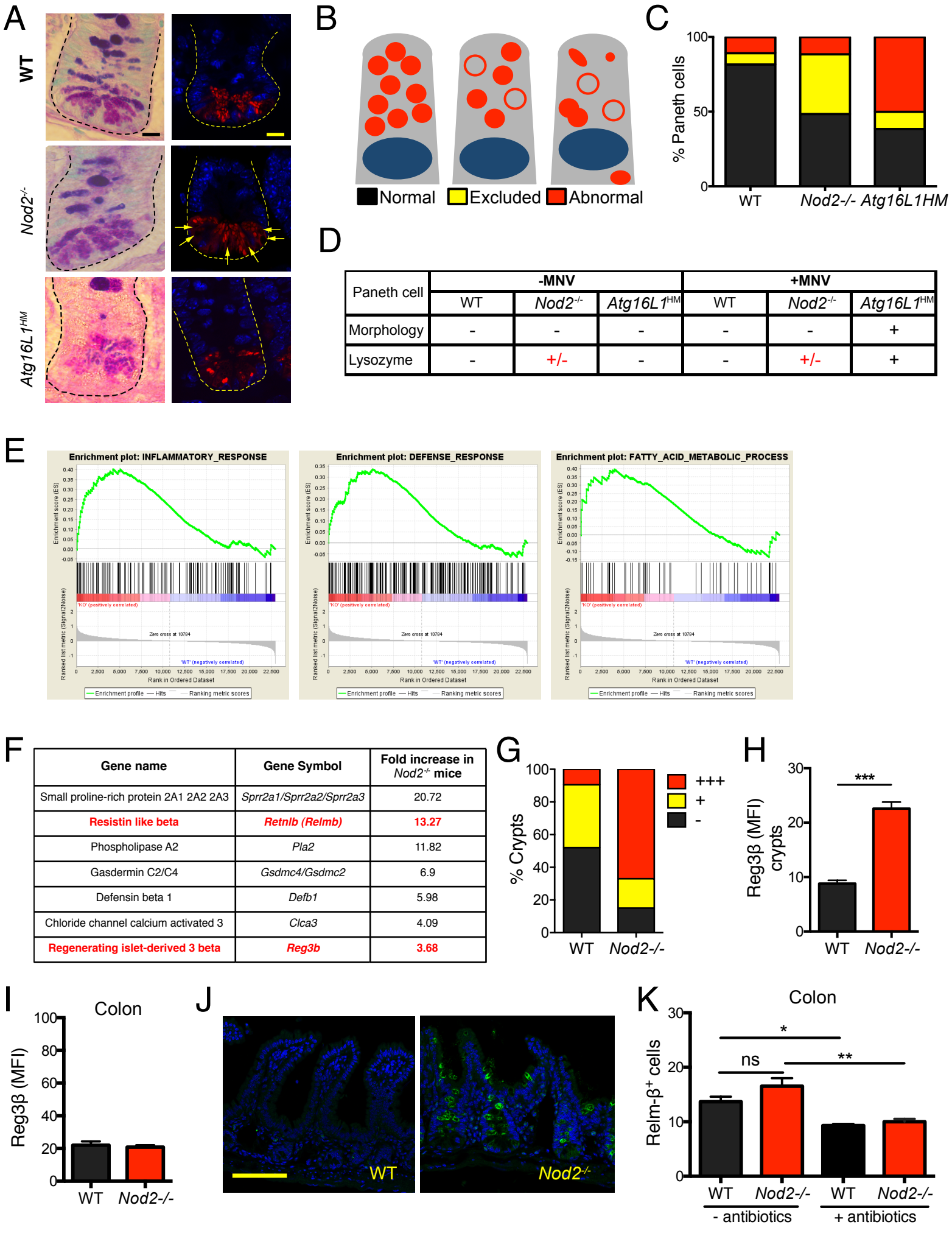
A
WT
Nod2-/-
Atg16L1HM
B
Normal
Excluded
Abnormal
C
% Paneth cells
100
50
0
WT
Nod2-/-
Atg16L1HM
D
Paneth cell
-MNV
+MNV
WT
Nod2-/-
Atg16L1HM
WT
Nod2-/-
Atg16L1HM
Morphology
- - - - - +
Lysozyme
- +/- - - +/- +
E
Enrichment plot: INFLAMMATORY_RESPONSE
Enrichment plot: DEFENSE_RESPONSE
Enrichment plot: FATTY_ACID_METABOLIC_PROCESS
Enrichment score (ES)
Ranked list metric (Signal2Noise)
'KO' (positively correlated)
Zero cross at 10784
'WT' (negatively correlated)
Rank in Ordered Dataset
Enrichment profile
Hits
Ranking metric scores
F
Gene name
Gene Symbol
Fold increase in Nod2-/- mice
Small proline-rich protein 2A1 2A2 2A3
Sprr2a1/Sprr2a2/Sprr2a3
20.72
Resistin like beta
Retnlb (Relmb)
13.27
Phospholipase A2
Pla2
11.82
Gasdermin C2/C4
Gsdmc4/Gsdmc2
6.9
Defensin beta 1
Defb1
5.98
Chloride channel calcium activated 3
Clca3
4.09
Regenerating islet-derived 3 beta
Reg3b
3.68
G
% Crypts
100
80
60
40
20
0
+++
+
-
WT
Nod2-/-
H
Reg3β (MFI) crypts
30
20
10
0
***
WT
Nod2-/-
I
Colon
Reg3β (MFI)
100
80
60
40
20
0
WT
Nod2-/-
J
WT
Nod2-/-
K
Colon
Relm-β+ cells
30
20
10
0
*
ns
**
WT
Nod2-/-
WT
Nod2-/-
- antibiotics
+ antibiotics

Figure S1, related to Figure 1. *Nod2*$^{-/-}$ mice display inflammatory gene expression in the epithelium rather than Paneth cell granule abnormalities.

(A-D) Mice with hypomorphic expression of *Atg16L1* (*Atg16L1*^{HM} mice) were previously shown to develop structural abnormalities in Paneth cells that were dependent on MNV infection (Cadwell et al., 2010). WT, *Nod2*$^{-/-}$ and *Atg16L1*^{HM} mice were either left untreated or infected with 3x10^{6} plaque forming units (pfu) of MNV CR6, and small intestinal sections were analyzed by light microscopy (PAS/alcian blue) and lysozyme immuno-fluorescence (IF) to compare Paneth cells as previously described (Cadwell et al., 2010). Representative images and quantification of MNV-infected samples are shown in (A) and (C), and the results are summarized in (D). (A) Only MNV-infected *Atg16L1*^{HM} mice develop Paneth cells with aberrant granule morphology by light microscopy. The amount of lysozyme^{+} structures was decreased overall in these samples, and those that were present were abnormally large or dysmorphic as previously described. Although the distribution of lysozyme was not as abnormal, some Paneth cells from *Nod2*$^{-/-}$ contained circular regions in which lysozyme was excluded (yellow arrows), similar to Crohn's disease patients with *Nod2* mutations (Vandussen et al., 2013). This "excluded" staining pattern was not dependent on MNV. Dotted lines denote crypt unit. (B) Illustrations depict the different types of lysozyme distribution that were observed. (C) Quantification of lysozyme distribution from (A). At least 100 Paneth cells from 3 mice were quantified per group. (D) Table summarizing results from (A) and (C).

(E) GSEA analysis of the microarray data from Figure 1 comparing gene expression in the small intestinal crypt-base epithelium of *Nod2*$^{-/-}$ and WT mice. Plots shown are examples of pathways associated with *Nod2*-deficiency (inflammatory response, defense response and fatty acid metabolic process pathways) and independently confirm the DAVID analysis. List of individual genes from the pathways shown are listed in Table S1.

(F) Genes displaying the highest increase in expression in *Nod2*$^{-/-}$ samples from the microarray.

(G-I) Additional IF analysis of Reg3β demonstrating that, compared to WT mice (G) almost all

small intestinal crypts in *Nod2*$^{-/-}$ mice displayed moderate (+) or high (+++) staining, (H) had an overall higher mean fluorescence intensity (MFI) in the small intestinal crypts and (I) no differences in MFI in the colon.

(J) Representative IF images of Relm-β^{+} expression in WT and *Nod2*$^{-/-}$ small intestine sections. **(K)** Quantification of Relm-β^{+} cells per 40X field in WT and *Nod2*$^{-/-}$ colon before and after treatment with antibiotics, confirming that the increase in Relm-β^{+} and Reg3β expression is limited to the small intestine, and overall expression of Relm-β is reduced in both WT and *Nod2*$^{-/-}$ colon treated with antibiotics, consistent with previous studies (Hill et al., 2010).

n ≥ 3 mice per genotype, *p<0.05, **p<0.01 and ***p<0.001 by unpaired two-tailed t test in (H) and Holm- Sidak multiple comparisons test in (K). Scale bar = 10μm in (A) and 100μm in (J). Data are represented as mean ± SEM in (H), (I) and (K).

FIGURE S2

A

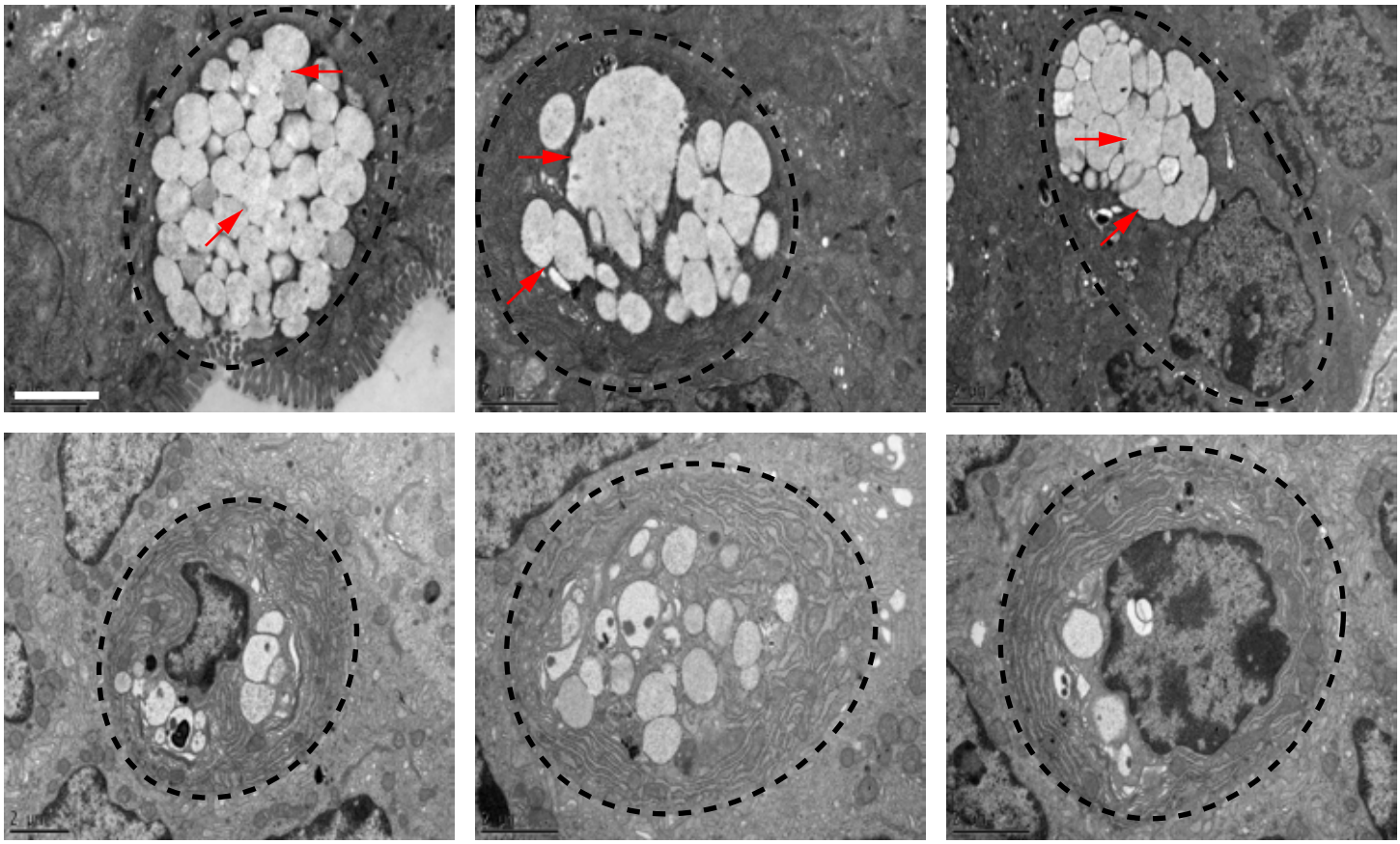

B

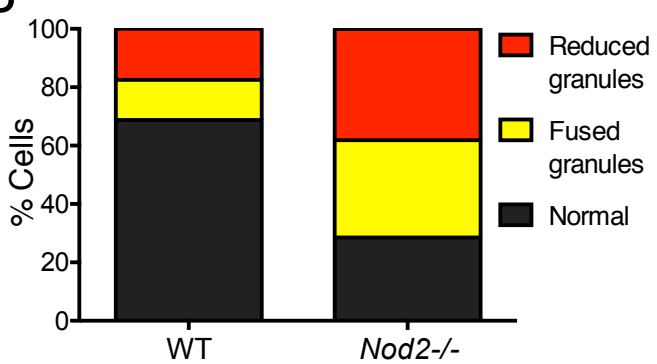
100
80
60
40
20
0
% Cells
WT
Nod2-/-
Reduced granules
Fused granules
Normal

Figure S2, related to Figure 2. Nod2-deficiency leads to goblet cell abnormalities.

(A) Representative images of goblet cells from *Nod2*$^{-/-}$ mice that display reduced number of granules or those with a fused appearance (red arrows). Scale bar = 2μm.

(B) Analysis of mucin granule morphology in WT and *Nod2*$^{-/-}$ goblet cells. Graph represents proportion of goblet cells in each genotype displaying granules with normal, reduced, or fused appearance. n = 3 mice per genotype.

Figure S3

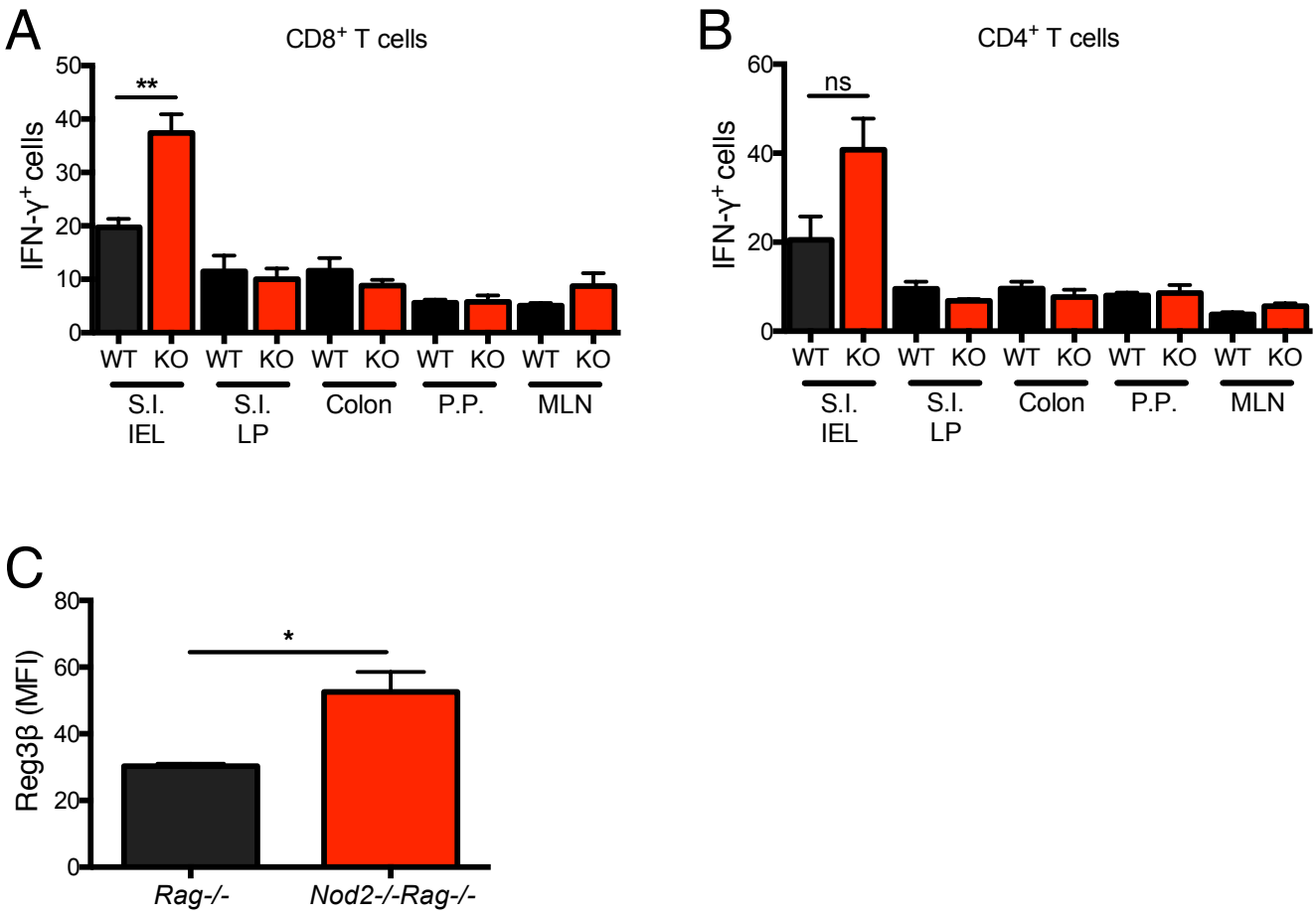
A
CD8+ T cells
IFN-γ+ cells
50
40
30
20
10
0
**
WT KO WT KO WT KO WT KO WT KO
S.I. IEL
S.I. LP
Colon
P.P.
MLN
B
CD4+ T cells
IFN-γ+ cells
60
40
20
0
ns
WT KO WT KO WT KO WT KO WT KO
S.I. IEL
S.I. LP
Colon
P.P.
MLN

C
Reg3β (MFI)
80
60
40
20
0
*
Rag-/-
Nod2-/-Rag-/-

Figure S3, related to Figure 3. Association between IFN-γ producing lymphocytes and epithelial abnormalities in *Nod2*$^{-/-}$ mice.

(A-B) In contrast to the increase in IFN-γ^{+} intraepithelial lymphocytes (IELs) observed in *Nod2*$^{-/-}$ mice, flow cytometry analysis indicates that WT and *Nod2*$^{-/-}$ mice have a similar proportion of IFN-γ^{+} CD8^{+} T cells (A) and CD4^{+} T cells (B) in the small intestinal lamina propria (LP), colon, Peyer's patches (P.P.), and mesenteric lymph nodes (MLN).

(C) IF analysis of Reg3β indicates a similar amount of staining in the small intestine of *Rag*$^{-/-}$ and *Nod2*$^{-/-}$*Rag*$^{-/-}$ mice.

n ≥ 3 mice per genotype. ns = not significant, *p<0.05 and **p<0.01 by unpaired two-tailed t test in (A), (B), and (C). Data are represented as mean ± SEM in (A), (B), and (C).

Figure S4

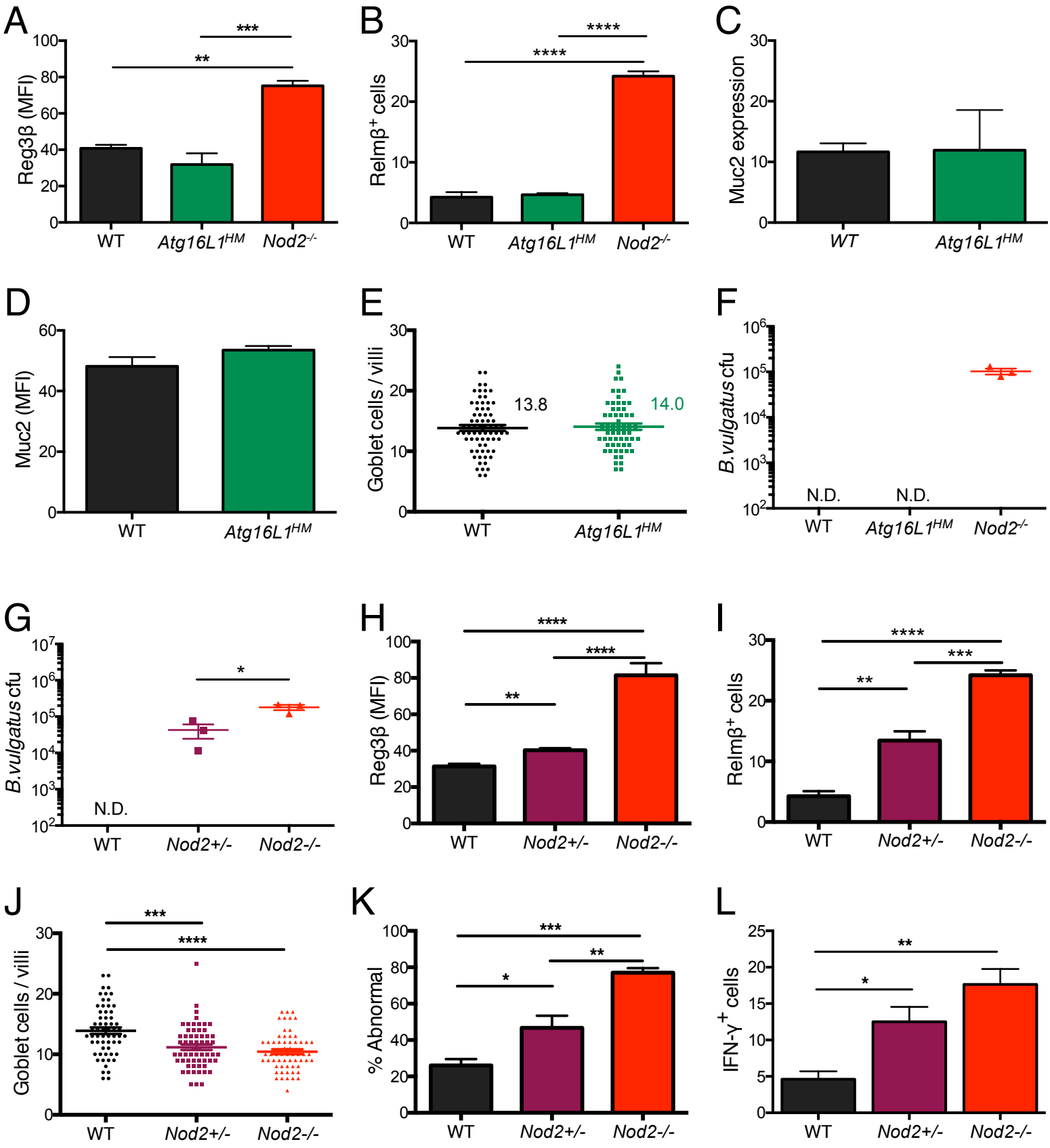
A
Reg3β (MFI)
WT
Atg16L1HM
Nod2-/-
B
Relmβ+ cells
C
Muc2 expression
D
Muc2 (MFI)
E
Goblet cells / villi
13.8
14.0
F
B.vulgatus cfu
N.D.
G
H
I
J
K
% Abnormal
L
IFN-γ+ cells
Nod2+/-

Figure S4, related to Figure 4. Intestinal abnormalities are specific to Nod2-deficiency.

(A-F) To demonstrate that the observed small intestinal abnormalities are specific to *Nod2*$^{-/-}$ mice, Atg16L1^{HM} mice were analyzed by quantifying (A) Reg3β expression by IF, (B) Relm-β^{+} cells per 40X field by IF, (C) *Muc2* expression normalized to *Gapdh* by qPCR, (D) Muc2 levels by IF, (E) number of goblet cells per villi by light microscopy, and (F) *B. vulgatus* cfu per mg of stool.

(G-L) To demonstrate a gene dosage effect, small intestinal abnormalities were analyzed in *Nod2*$^{+/-}$ mice by quantifying (G) *B. vulgatus* cfu per mg of stool, (H) Reg3β expression by IF, (I) Relm-β^{+} cells per 40X field by IF, (J) goblet cell numbers and (K) proportion displaying abnormal morphology by light microscopy, and (L) the proportion of IFNγ^{+}CD8^{+} IELs by flow cytometry.

n ≥ 3 mice per genotype. *p<0.05, **p<0.01, ***p<0.001 and ****p<0.0001 by ANOVA followed by Holm-Sidak multiple comparison test for (A), (B), (H), (I), (J), (K), and (L) and unpaired two-tailed t test in (C), (D), (E) and (G). Data are represented as mean ± SEM in (A), (B), (C), (D), (E), (G), (H), (I), (K), and (L). Data represents mean in (E) and (J).

Figure S5

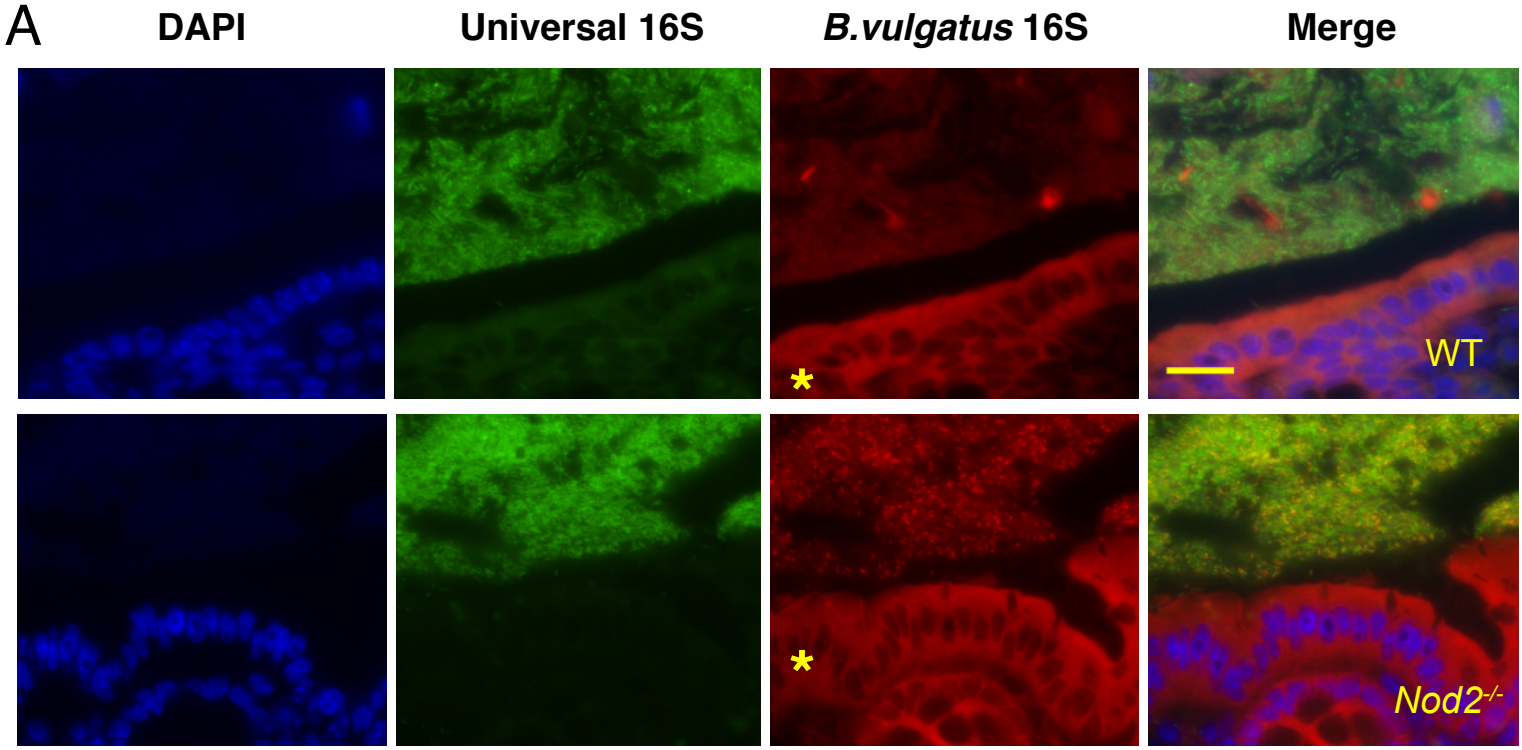

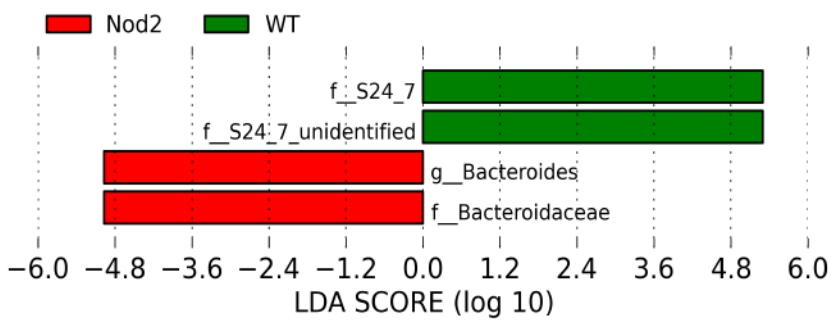

C

	WT	*Nod2-/-*
Bacteroides vulgatus	0	12
Bacteroides acidophilus	3	0
Bacteroides eggerthii	2	0
Parabacteroides goldstenii	3	0
No *Bacteroides* growth	4	0

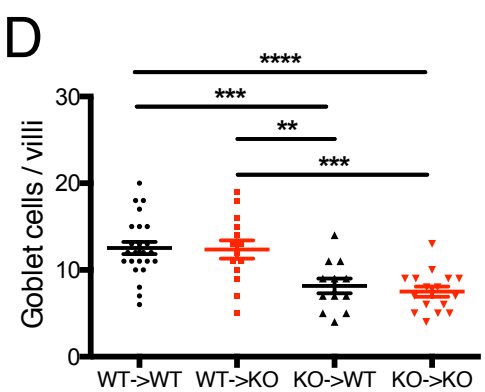

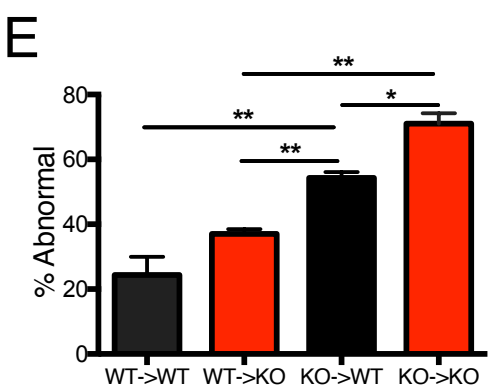

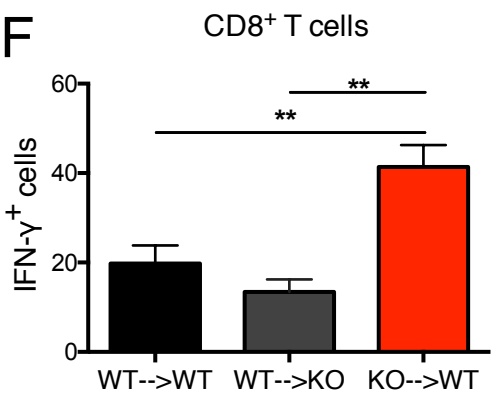

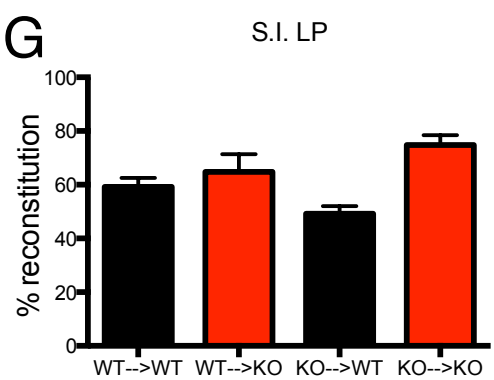

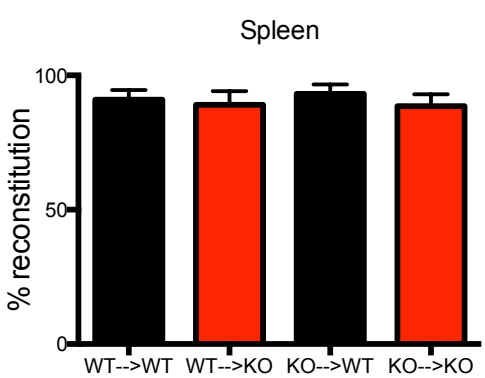

Figure S5, related to Figure 5. Nod2-deficiency in the hematopoietic compartment is responsible for intestinal abnormalities induced by *B. vulgatus*.

(A) Small intestine and colon were analyzed by fluorescent *in situ* hybridization (FISH) using probes complimentary to either universal (green) or *B. vulgatus*-specific (red) 16S rRNA. DAPI is shown in blue. *B. vulgatus* was only detected in the small intestine and colon of *Nod2*$^{-/-}$ mice, and was restricted to the lumen. Representative images of the colon from 3 mice per genotype are shown. Yellow asterisks refers to non-specific binding of the *B.vulgatus* 16S probe to intestinal tissue (Scale bar = 20μm).

(B) Supervised analysis with LEfSe (logarithmic LDA threshold score of 4.8) found the *Bacteroides* genus to be differentially enriched in *Nod2*$^{-/-}$ mice, while the family S24-7 were differentially enriched in WT mice.

(C) Stool from 12 WT and 12 *Nod2*$^{-/-}$ mice were plated on BBE agar and the colony forming species were identified by sequencing of the 16S rRNA gene. Upon co-housing WT and *Nod2*$^{-/-}$ mice, we were able to transfer *B. vulgatus* to WT mice (Figure 5F), but were unable to transfer other *Bacteroides* species from WT mice to *Nod2*$^{-/-}$ mice.

(D-G) Small intestinal abnormalities in bone marrow chimeras from Figure 5F (donor --> recipient) were analyzed by quantifying (D) goblet cell numbers, (E) proportion of goblet cells displaying abnormal morphology, (F) the number of IFNγ^{+}CD8^{+} IELs by flow cytometry. An insufficient number of viable IELs were harvested from the KO→KO condition to allow flow cytometric analysis. (G) Chimerism determined by flow cytometry analysis of congenic markers CD45.1 (WT, Jackson Laboratories) and CD45.2 (*Nod2*$^{-/-}$) in small intestinal L.P. and spleen. Reg3β levels could not be assessed in chimeric mice because the procedure of generating the mice induced high levels, most likely due to the damage caused by irradiation. $n \geq 9$ mice per group. *$p<0.05$, **$p<0.01$, ***$p<0.001$ and ****$p<0.0001$ by ANOVA followed by Holm-Sidak multiple comparison test for (D), (E), and (F). Data are represented as mean ± SEM in (D), (E), (F) and (G).

Figure S6

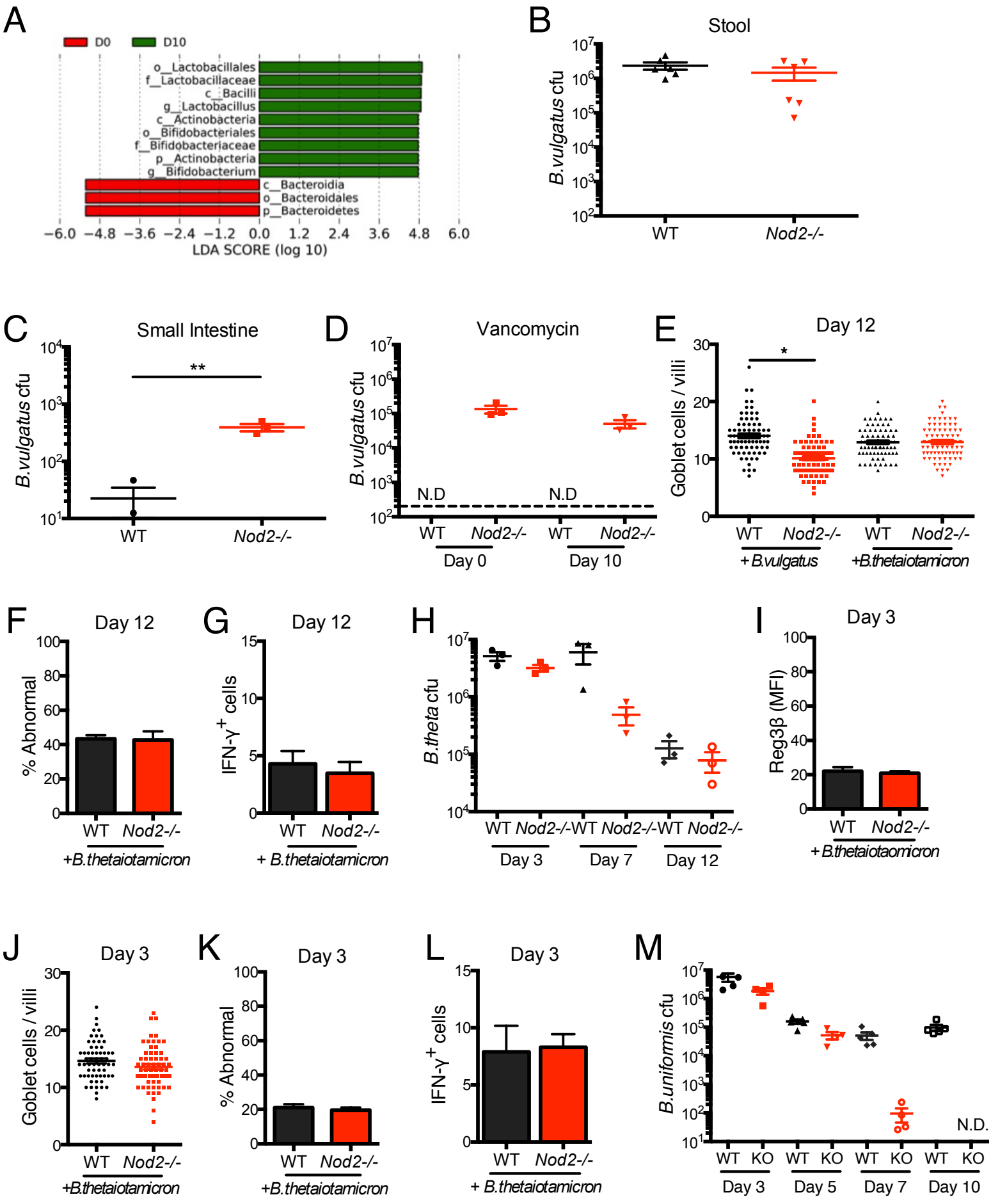
A
D0
D10
o__Lactobacillales
f__Lactobacillaceae
c__Bacilli
g__Lactobacillus
c__Actinobacteria
o__Bifidobacteriales
f__Bifidobacteriaceae
p__Actinobacteria
g__Bifidobacterium
c__Bacteroidia
o__Bacteroidales
p__Bacteroidetes
−6.0 −4.8 −3.6 −2.4 −1.2 0.0 1.2 2.4 3.6 4.8 6.0
LDA SCORE (log 10)
B
Stool
B.vulgatus cfu
WT
Nod2-/-
C
Small Intestine
B.vulgatus cfu
**
WT
Nod2-/-
D
Vancomycin
B.vulgatus cfu
N.D
N.D
WT Nod2-/- WT Nod2-/-
Day 0
Day 10
E
Day 12
Goblet cells / villi
*
WT Nod2-/- WT Nod2-/-
+B.vulgatus
+B.thetaiotamicron
F
Day 12
% Abnormal
WT Nod2-/-
+B.thetaiotamicron
G
Day 12
IFN-γ+ cells
WT Nod2-/-
+ B.thetaiotamicron
H
B.theta cfu
WT Nod2-/- WT Nod2-/- WT Nod2-/-
Day 3
Day 7
Day 12
I
Day 3
Reg3β (MFI)
WT Nod2-/-
+B.thetaiotaomicron
J
Day 3
Goblet cells / villi
WT Nod2-/-
+B.thetaiotamicron
K
Day 3
% Abnormal
WT Nod2-/-
+B.thetaiotamicron
L
Day 3
IFN-γ+ cells
WT Nod2-/-
+ B.thetaiotamicron
M
B.uniformis cfu
N.D.
WT KO WT KO WT KO WT KO
Day 3
Day 5
Day 7
Day 10

Figure S6, related to Figure 6. *Nod2*$^{-/-}$ mice are susceptible to *B. vulgatus* but not *B. thetaiotamicron*.

(A) Supervised analysis with LEfSe showing *Bacteroides* genus to be differentially enriched in *Nod2*$^{-/-}$ mice on Day 0 of metronidazole treatment, while *Lactobacillus* and *Bifidobacteria* were differentially enriched in *Nod2*$^{-/-}$ mice on Day 10 after metronidazole treatment.

(B) To demonstrate successful reconstitution, *B. vulgatus* levels were quantified in stool on day 12 post-inoculation from mice that were first depleted of the bacteria by metronidazole-treatment and then gavaged with 10^8 cfu.

(C) In contrast to the similar amount of *B. vulgatus* in the stool of WT and *Nod2*$^{-/-}$ mice following reconstitution, there were significantly higher amounts recovered from the of *Nod2*$^{-/-}$ small intestinal mucosa. To quantify tissue-associated bacteria in (C), 2 cm of the small intestine (ileum) was flushed with PBS, homogenized, and serial dilutions were plated on *Bacteroides* Bile Esculin agar under anaerobic conditions.

(D) Quantification of *B. vulgatus* in stool of WT and *Nod2*$^{-/-}$ mice on day 0 and 10 after vancomycin treatment demonstrating lack of depletion.

(E) Quantification of goblet cell numbers in WT and *Nod2*$^{-/-}$ mice, 12 days post gavage with *B. vulgatus* or *B. thetaiotaomicron* following metronidazole treatment.

(F) Quantification of the proportion of goblet cells displaying abnormal morphology in WT and *Nod2*$^{-/-}$ mice, 12 days post gavage with *B. thetaiotaomicron* following metronidazole treatment.

(G) Flow cytometry analysis of the number of IFN-γ^+ IELs in WT and *Nod2*$^{-/-}$ mice, 12 days post gavage with *B. thetaiotaomicron* following metronidazole treatment.

(H) WT and *Nod2*$^{-/-}$ mice were treated with metronidazole and then gavaged with 10^8 cfu of *B. thetaiotaomicron*. Quantification of *B. thetaiotaomicron* in stool on indicated days indicate that colonization is sustained.

(I-L) Quantification of Reg3β expression by IF (I), goblet cell numbers (J) and proportion displaying abnormal morphology (K), and IFN-γ^+ IELs in WT and *Nod2*$^{-/-}$ mice (L), 3 days post

gavage with *B. thetaiotaomicron* following metronidazole treatment.

(M) WT and *Nod2*$^{-/-}$ mice were treated with metronidazole and then gavaged with 10^8 cfu of *B. uniformis*. Quantification of *B.uniformis* cfu in stool indicates that stable colonization is sustained 10 days post gavage in WT mice but not *Nod2*$^{-/-}$ mice.

n ≥ 3 mice per genotype. *p<0.05 by ANOVA followed by Holm-Sidak multiple comparison test for (E) and unpaired two-tailed T test for (B), (D), (F), (G), (I), (J), (K) and (L). Data are represented as mean ± SEM in (B), (C), (D), (F), (G), (H), (I), (K), (L), and (M). Bar represents mean in (E) and (J).

FIGURE S7

A

B

	Piroxicam only		+Metronidazole		+Metronidazole +*B.vulgatus*	
	WT	*Nod2*$^{-/-}$	WT	*Nod2*$^{-/-}$	WT	*Nod2*$^{-/-}$
Intestinal bleeding	0/5 0%	3/4 75%	0/5 0%	0/5 0%	0/5 0%	3/5 60%
Attachment to cavity	0/5 0%	3/4 75%	0/5 0%	0/5 0%	0/5 0%	3/5 60%

C

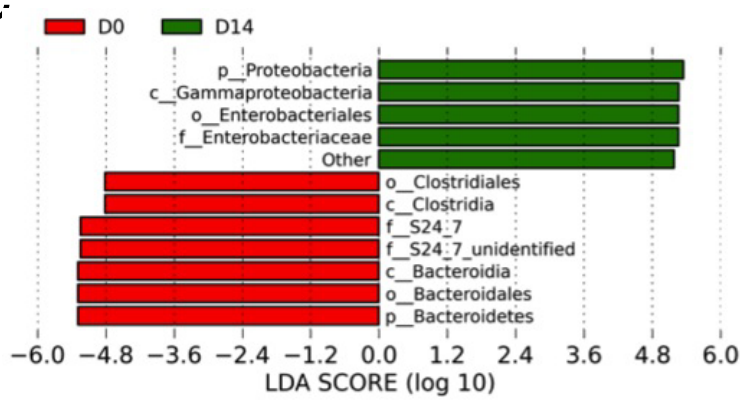

D

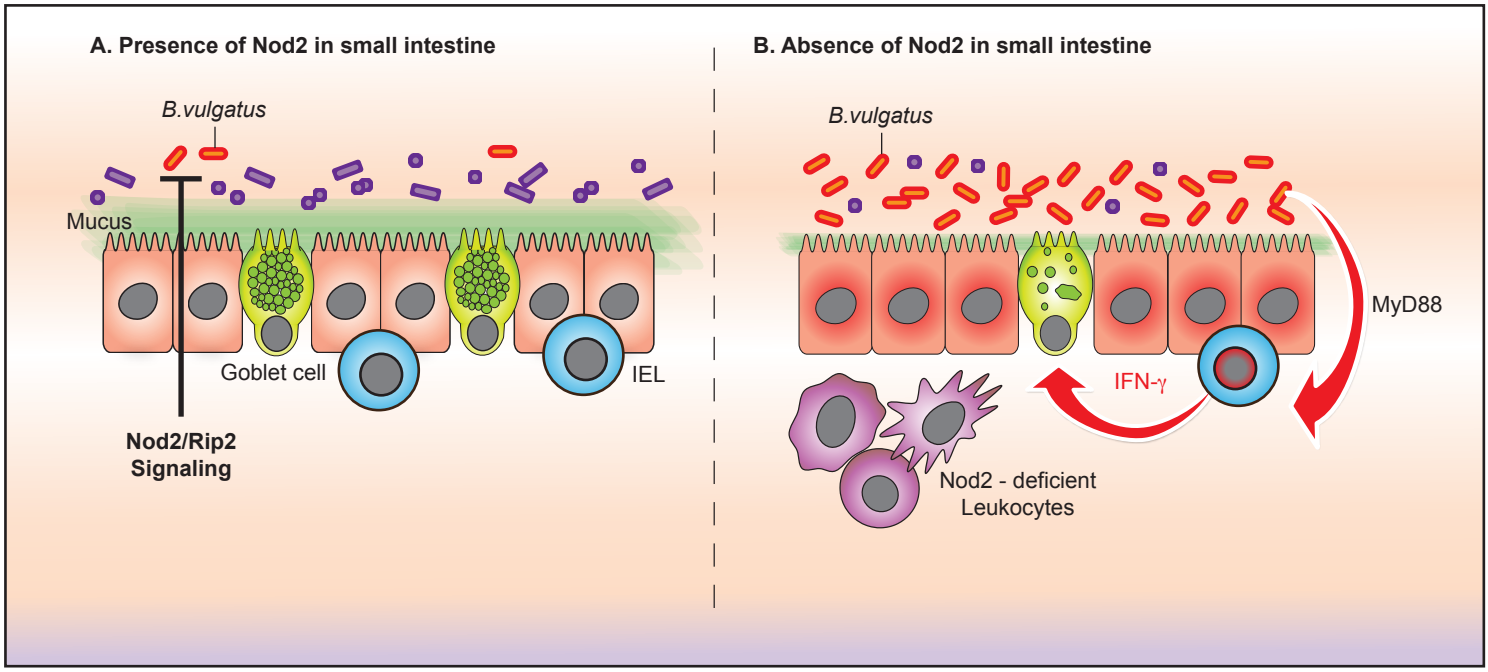

Figure S7, related to Figure 7. *Nod2*$^{-/-}$ mice display exacerbated inflammatory pathologies and dysbiosis following piroxicam treatment.

(A) Representative image of intestinal bleeding (asterisk) and attachment of the ileal-cecal junction to the surrounding tissue of the peritoneal cavity (arrow) that was observed only in *Nod2*$^{-/-}$ mice harboring *B. vulgatus*.

(B) Table representing quantification of small intestinal bleeding and attachment of the intestine to the peritoneal cavity in piroxicam-treated WT and *Nod2*$^{-/-}$ mice receiving no other treatment (piroxicam only), metronidazole, or metronidazole followed by gavage with 10^8 *B.vulgatus*.

(C) Supervised analysis with LEfSe showing that the intestinal microbiota profile of *Nod2*$^{-/-}$ mice on day 0 of piroxicam treatment was dominated by the phylum *Bacteroidetes*, while the intestinal microbiota profile of *Nod2*$^{-/-}$ mice at day 14 of piroxicam treatment was dominated by the phylum *Proteobacteria*.

(D) The presence of Nod2 in myeloid or dendritic cell types provides Rip2-mediated gene expression that favors microbial resistance and immune homeostasis in the small intestine. In the absence of Nod2, there is decreased microbial resistance to the pro-inflammatory commensal *B. vulgatus*, which promotes a Myd88-dependent inflammatory reaction. This adverse response to *B. vulgatus* includes excess IFN-γ production by intraepithelial lymphocytes that causes defects in mucus production by goblet cells, and allows sustained colonization by *B. vulgatus* and susceptibility to disease.

Supplemental Experimental Procedures

qRT-PCR. For quantifying gene expression, total RNA was isolated from small intestinal tissue using Trizol and chloroform and the Protoscript cDNA synthesis kit (NEB) was used to synthesize and amplify cDNA. Relative expression of muc2 (Fwd 5'-ATGCCCACCTCCTCAAAGAC-3', Rev 5'-GTAGTTTCCGTTGGAACAGTGAA-3') and α-defensin1 (Fwd 5'-AAGAGACTAAAACTGAGGAGCAGC-3', Rev 5'-GGTGATCATCAGACCCCAGCATCAGT-3') were normalized to GAPDH (Fwd 5'-TGCCCCCATGTTTGTGATG-3', Rev 5'-TGTGGTCATGAGCCCTTCC-3'). For quantifying bacteria, DNA was isolated from tissue or stool samples using phenol chloroform. *Bacteroides* 16S (Fwd 5'-GAGAGGAAGGTCCCCCAC-3', Rev 5'-CGCTACTTGGCTGGTTCAG-3') was normalized to total 16S using universal primers (Fwd 5'- ACTCCTACGGGAGGCAGCAGT-3', Rev 5'-ATTACCGCGGCTGCTGGC-3'). qRT-PCR was done using SyBr Green master mix (Roche) and Light Cycler 480 (Roche).

Transmission electron microscopy (TEM). Small intestinal sections from WT and *Nod2*$^{-/-}$ mice were fixed in 2.5% glutaraldehyde, and 2% paraformaldehyde in 0.1M sodium cacodylate buffer (pH 7.2) for 2 hours and post-fixed with 1% osmium tetroxide for 1.5 hours at room temperature, then processed in a standard manner and embedded in EMbed 812 (Electron Microscopy Sciences, Hatfield, PA). Semi-thin sections were cut at 500nm and stained with 1% toluidine blue to evaluate the quality of preservation. Ultrathin sections (60 nm) were cut, mounted on copper grids and stained with uranyl acetate and lead citrate by standard methods. Stained grids were examined under Philips CM-12 electron microscope (FEI; Eindhoven, The Netherlands) and photographed with a Gatan (4k x2.7k) digital camera (Gatan, Inc., Pleasanton, CA).

Fluorescent *in situ* hybridization (FISH). Small intestine and colonic sections were prepared by fixing whole tissue including the lumen in methacarn at 4^{o}C followed by paraffin embedding. 5μm thick sections were hybridized to a universal bacterial probe EUB 338 (FITC - GCTGCCTCCCGTAGGAGT) and a probe specific for *B.vulgatus* 16S rRNA (Alexa 594 - AGATGCCTTGCGGCTTACGGC) in 10% formamide, 2X sodium saline citrate and 10% SDS at 37^{o}C overnight. Non-specific probes were designed and used as controls for both probes. Sections were imaged using the Applied Precision personal DV system.

Flow cytometry. To obtain lymphocytes from Peyer's patches and MLNs, the tissue was collected and homogenized using a 40μm filter and washed with RPMI. Lymphocytes were stimulated for 4 hours with a cell stimulation cocktail of PMA, ionomycin, brefeldin A and monensin from eBioscience. Stimulated cells were stained with anti-CD3ε PerCP, anti-TCRβ PE-Cy5, anti-CD8α PE-Cy7, anti CD4 APC-Cy7, anti-IFNγ APC and their respective isotype controls from Biolegend, and, anti-IL-17 PE, anti-TCRδ FITC and their respective isotype controls from BD. Fixation and permeabilization buffers from Biolegend were used for intracellular cytokine staining, and a fixable live/dead stain from BD was used to exclude dead cells. Flow cytometric analysis was performed on an LSR II (BD biosciences) and analyzed using FlowJo software from TreeStar.

16S rRNA sequencing, QIIME, and LEfSe analyses. DNA isolation from stool samples was done using the NucleospinSoil Kit (Macherey-Nagel). Bacterial 16S rRNA gene was amplified at the V4 region using a modified protocol from Kuczyniski et al (Kuczynski et al., 2011) and paired-end amplicon sequencing was performed on the Illumina MiSeq system. Sequencing reads were processed using the Quantitative Insights Into Microbial Ecology (QIIME) software package. Operational taxonomic units (OTUs) were identified using a combination of closed-reference and de novo clustering methods. Beta diversity was calculated using unweighted UniFrac distance (Chen et al., 2012; Lozupone et al., 2011) on an uneven OTU table. Principle Coordinate Analysis (PCoA) was performed on the unweighted UniFrac distance matrix and visualized with the KiNG graphics program. Alpha diversity was calculated using the metrics Shannon index [ref] and observed species. The LDA Effect Size (LEfSe) algorithm (http://huttenhower.sph.harvard.edu/galaxy/) was used to identify taxa that were differentially abundant in different biological groups (Segata and Huttenhower, 2011).

Supplemental References

Cadwell, K., Patel, K.K., Maloney, N.S., Liu, T.C., Ng, A.C., Storer, C.E., Head, R.D., Xavier, R., Stappenbeck, T.S., and Virgin, H.W. (2010). Virus-plus-susceptibility gene interaction determines Crohn's disease gene Atg16L1 phenotypes in intestine. Cell *141*, 1135-1145.

Chen, J., Bittinger, K., Charlson, E.S., Hoffmann, C., Lewis, J., Wu, G.D., Collman, R.G., Bushman, F.D., and Li, H. (2012). Associating microbiome composition with environmental covariates using generalized UniFrac distances. Bioinformatics *28*, 2106-2113.

Hill, D.A., Hoffmann, C., Abt, M.C., Du, Y., Kobuley, D., Kirn, T.J., Bushman, F.D., and Artis, D. (2010). Metagenomic analyses reveal antibiotic-induced temporal and spatial changes in intestinal microbiota with associated alterations in immune cell homeostasis. Mucosal immunology *3*, 148-158.

Kuczynski, J., Stombaugh, J., Walters, W.A., Gonzalez, A., Caporaso, J.G., and Knight, R. (2011). Using QIIME to analyze 16S rRNA gene sequences from microbial communities. Current protocols in bioinformatics / editoral board, Andreas D Baxevanis [et al] *Chapter 10*, Unit 10 17.

Lozupone, C., Lladser, M.E., Knights, D., Stombaugh, J., and Knight, R. (2011). UniFrac: an effective distance metric for microbial community comparison. The ISME journal *5*, 169-172.
Segata, N., and Huttenhower, C. (2011). Toward an efficient method of identifying core genes for evolutionary and functional microbial phylogenies. PLoS One *6*, e24704.

Vandussen, K.L., Liu, T.C., Li, D., Towfic, F., Modiano, N., Winter, R., Haritunians, T., Taylor, K.D., Dhall, D., Targan, S.R*., et al.* (2013). Genetic Variants Synthesize to Produce Paneth Cell Phenotypes That Define Subtypes of Crohn's Disease. Gastroenterology.